Biochemical and Biophysical Research Communications 463 (2015) 587–592

Contents lists available at ScienceDirect

Biochemical and Biophysical Research Communications

journal homepage: www.elsevier.com/locate/ybbrc

Sub-cellular force microscopy in single normal and cancer cells

H. Babahosseini [a, 1], B. Carmichael [b, 1], J.S. Strobl [a], S.N. Mahmoodi [b, *], M. Agah [a, *]

[a] VT MEMS Laboratory, The Bradley Department of Electrical and Computer Engineering, Blacksburg, VA 24061, USA
[b] Nonlinear Intelligent Structures Laboratory, Department of Mechanical Engineering, University of Alabama, Tuscaloosa, AL 35487-0276, USA

ARTICLE INFO

Article history:
Received 14 May 2015
Accepted 28 May 2015
Available online 31 May 2015

Keywords:
Sub-cellular biomechanics
Generalized Maxwell model
Atomic force microscope (AFM)
Human breast cells

ABSTRACT

This work investigates the biomechanical properties of sub-cellular structures of breast cells using atomic force microscopy (AFM). The cells are modeled as a triple-layered structure where the Generalized Maxwell model is applied to experimental data from AFM stress-relaxation tests to extract the elastic modulus, the apparent viscosity, and the relaxation time of sub-cellular structures. The triple-layered modeling results allow for determination and comparison of the biomechanical properties of the three major sub-cellular structures between normal and cancerous cells: the up plasma membrane/actin cortex, the mid cytoplasm/nucleus, and the low nuclear/integrin sub-domains. The results reveal that the sub-domains become stiffer and significantly more viscous with depth, regardless of cell type. In addition, there is a decreasing trend in the average elastic modulus and apparent viscosity of the all corresponding sub-cellular structures from normal to cancerous cells, which becomes most remarkable in the deeper sub-domain. The presented modeling in this work constitutes a unique AFM-based experimental framework to study the biomechanics of sub-cellular structures.

1. Introduction

Atomic force microscopy (AFM) is an established method for tissue-level and single-cell biomechanical characterization. Several studies have shown that transformed cells are generally softer and more deformable than their healthier counterparts which can facilitate their motility and metastasis [1]. Particularly for breast epithelial cells, AFM results have shown that the highly metastatic MDA-MB-231 cell line is significantly more deformable than the non-tumorigenic MCF10A cells [2,3]. Experimentally, agents that increase cell stiffness decrease breast cancer invasiveness, providing evidence for a direct relationship between the metastatic potential of cancer cells and their mechanical properties [4]. Several articles have also revealed that time-dependent viscoelastic properties can also serve as indicators of cell disease [5]. The determination of viscoelastic properties has been done by implementing stress-relaxation test using different techniques, particularly AFM [5,6]. Meanwhile, the network of cytoskeletal proteins and the nucleus have been found to play the most significant role in determining the biomechanical properties of cells [7].

To determine single cell representative biomechanical properties, the generated experimental data are typically analyzed through the Hertz model and its extension into the time domain, the Standard Linear Solid (SLS) model [8–10]. Different research groups have used this approach to introduce cell biomechanical properties as “label-free” biophysical markers to predict cancer risk, cancer progression from benign to aggressive stages [32], and treatment efficacy [33]. Despite promising results, the current trend in single-cell force microscopy does not provide the most comprehensive and information-rich picture of cell biomechanics. The use of the SLS model for quantification of cell biomechanical properties assumes that the cell is an entirely homogenous material, ignores the cell's complex multi-layered architecture, and neglects the cell's nonlinear depth-dependent elastic and viscoelastic properties [11–13,34]. Moreover, the indentation depth for cell measurements is typically kept below 10% of a cell thickness to keep the validity of the assumptions and to avoid possible error introduced by deformation nonlinearity and substrate contributions [14]. However, there is growing evidence in the literature that this limitation is too conservative and contributions from the substrate are negligible up to 50% of the cell thickness [15,16], overlooking detailed information about the cell mechanics in deeper layers of the cells [17].

The Generalized Maxwell (GM), a more advanced viscoelastic model has been successfully applied to relaxation measurements of

* Corresponding authors.
E-mail addresses: nmahmoodi@eng.ua.edu (S.N. Mahmoodi), agah@vt.edu (M. Agah).
[1] Both authors equally contributed to this work.

http://dx.doi.org/10.1016/j.bbrc.2015.05.100
0006-291X/

biological samples [18–20]. This model incorporates the idea of multiple relaxation times, and therefore, it can provide insight about the transient response of sub-cellular structures to external mechanical stimuli by distributing the response across several time scales. Consequently, the model leads to more extensive parameter sets to characterize and analyze the biomechanical properties of cell components. There have been only a few studies based on the GM model for characterizing cell viscoelastic properties by AFM nano-indentation [21,22], however the comparison of the biomechanical characterization of the sub-cellular structures among normal and cancerous cells has been left untouched.

This paper reports the biomechanical properties of sub-cellular structures of breast carcinoma MDA-MB-231 and benign MCF10A cells. For this purpose, stress-relaxation AFM tests are conducted on single cells after applying a deep probe indentation (up to 50% of cell height), and the resulting experimental data are analyzed with the GM viscoelastic model.

2. Materials and methods

2.1. Cell culture and sample preparation

MCF10A and MDA-MB-231 breast cell lines representative of non-invasive and highly invasive breast cancer models, respectively, were purchased from the American Type Culture Collection (ATCC). The cells were maintained in plastic T-25 cm^2 culture flasks in standard cell culture medium presented in Refs. [2,3]. For the AFM tests, the cells were harvested and then seeded at a density of 1×10^5 cells per 12 mm^2 glass coverslips coated with 0.1 mg/mL collagen type IV (Sigma–Aldrich, St. Louis, MO) for 24–30 h at 37 °C in humidified 7% CO_2-93% air atmosphere prior to the AFM experiments to allow the cells to adhere. A buffered HEPES solution was then added to the coverslip samples (final concentration of 13.5 mM) to maintain a physiological pH of 7.2 during testing.

2.2. Scanning electron microscopy (SEM)

SEM was performed to investigate morphology and the height for both cell lines on the surface. The cells were fixed in 3.7% formaldehyde in PBS for 10 min, 24–30 h after plating on collagen-coated coverslips. The samples were critical-point-dried to eliminate changes in the cell morphology, sputter-coated with a thin layer of gold palladium, and mounted on an SEM sample holder using conductive tape prior to the SEM imaging. To approximate the cells height, the SEM images were acquired with 85° tilt of the sample stage to allow a side-view visualization. The images were obtained using a Leo ZEISS 1550 field-emission SEM instrument.

2.3. Atomic force microscopy (AFM)

The AFM experiments were performed with a Dimension Icon AFM with a closed loop controller (Bruker Corporation, Billerica, MA) integrated with an optical microscope. Olympus TR400PSA V-shaped SiNi cantilevers (Olympus, Tokyo, Japan) of ~200 μm length with approximate spring constant values of ~0.02 N/m were employed in all AFM experiments; exact spring constant values were measured via the thermal tuning method. The sharp probes were modified by attaching glass spheres (Duke Scientific, Waltham, MA) of ~10 μm diameter onto the cantilever free end with two-part epoxy (Miller Stephenson, Sylmar CA), which helped reduce damage to the cells due to contact. The exact diameter of the glass sphere and its attachment location were identified using a HIROX KH-7700 3D Digital Video Microscope. The measurements were carried out on single cells in their respective culture medium at room temperature (24 °C) using AFM contact mode. The indentations were done above each cell's nucleus under optical control. Stress-relaxation test corresponding to each cell response to a unit step displacement was implemented [10] to acquire stress-relaxation curves for a total period of 60 s at a 5 kHz sample rate and a constant high approach velocity of 5 μm/s to approximate a pure step displacement. A maximum force trigger of 30 nN was implemented for all curve acquisition, leading to a deep indentation of about 3 μm on the cells, which are sufficient to probe the membrane and the underlying cytoplasm and nucleus [23].

2.4. Generalized Maxwell viscoelastic model

One model that has been successfully applied to AFM stress-relaxation experiments on biological samples is the Generalized Maxwell (GM) model [18–20]. The GM model is similar in form to the Standard Linear Solid (SLS) model which was previously widely employed [8–10], but incorporates the concept of multiple relaxation times corresponding to a larger number of viscous elements. A helpful visualization is an arrangement of stacked viscous balls of increasing viscosity. As shown in Fig. 1A, an applied force would quickly deform the less viscous element, which would slowly relax. The more viscous elements, however, would quickly snap back to their initial shape due to the larger restoring force. The same is true for sub-structures of heterogeneous composition. A parallel representation of the elements effectively represents the same effect but distributes the response across the time domain. Fig. 1B shows the representative mechanical system of the GM model, where the subscript on the parameters denotes the branch in the parallel structure. The equations of motion for the system may be written compactly:

$$\sigma = \left(E_R + \frac{E_1\mu_1\mathscr{D}}{E_1+\mu_1\mathscr{D}} + \cdots + \frac{E_n\mu_n\mathscr{D}}{E_n+\mu_n\mathscr{D}}\right)\varepsilon\,, \tag{1}$$

where E_R is the relaxed modulus, E_n is the n-th elastic coefficient, μ_n is the n-th viscous coefficient, and $\mathscr{D}$ is the differential operator such that $\mathscr{D}^n(\cdot) = d^n/dt^n(\cdot)$. A transformation into the Laplace domain results in the ratio of stress to strain equation:

$$\frac{\overline{\sigma}}{\overline{\varepsilon}} = K(s) = \left(E_R + \frac{E_1\mu_1 s}{E_1+\mu_1 s} + \cdots + \frac{E_n\mu_n s}{E_n+\mu_n s}\right). \tag{2}$$

Through the analogous modulus of rigidity, a time-dependent elastic modulus may be expressed in the Laplace domain as:

$$\overline{E}(s) = (1+\nu)\,K(s). \tag{3}$$

The relation between an applied normal force, F, by a spherical body with radius, R, and a sample deformation, δ, with Poisson's ratio, ν and elastic modulus, E, can be expressed by the Hertz model [24] as follows:

$$F = \frac{4E\sqrt{R}}{3(1-\nu^2)}\delta^{\frac{3}{2}} \tag{4}$$

Assuming that the initial contact force is applied constantly throughout the relaxation, it may be modeled as a Heaviside function. Eq. (4) may then be extended into the Laplace domain by replacing elastic modulus with the result of Eq. (3):

$$\overline{F}(s) = \frac{4}{3}\frac{\sqrt{R\delta_0^3}}{(1-\nu)}\frac{K(s)}{s}, \tag{5}$$

where δ_0 is the maximum indentation resulting from the application of the contact force. Substitution of Eq. (2) into Eq. (5) and

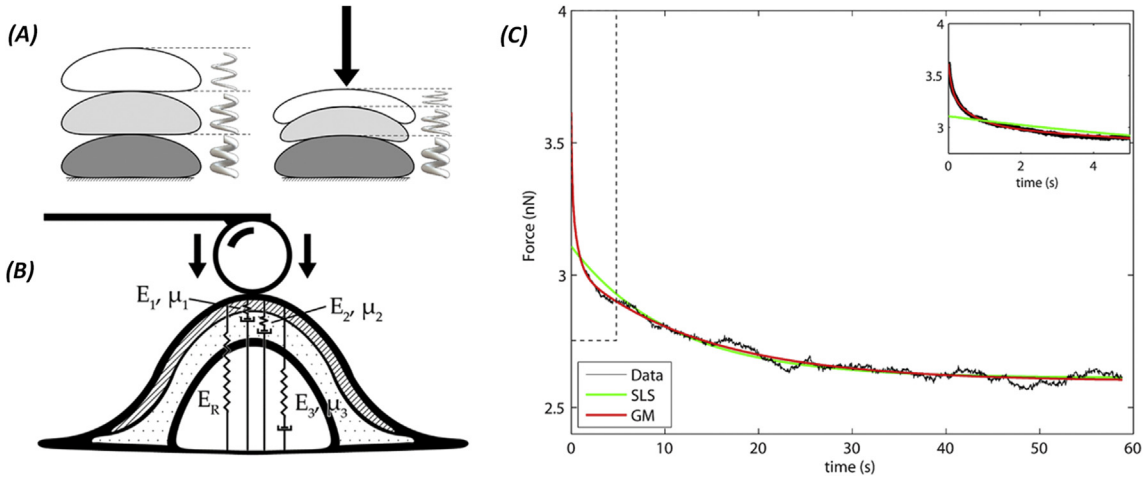

Fig. 1. (A) An illustration of a triple-layered structure before and after load application. The higher restoring force of the more viscous element would quickly correct the deflection, while the less viscous element would require much more time. (B) Mechanical Schematic of the Generalized Maxwell model of a cell. (C) Comparison of experimental data and the SLS and the GM fits with a highlighted difference in the initial cell response fitting.

transformation back into the time domain show the contribution of the multiple branches:

$$F(t) = \frac{4}{3}\frac{\sqrt{R\delta_0^3}}{(1-\nu)}\left[E_R + E_1 e^{-\frac{E_1}{\mu_1}t} + \cdots + E_n e^{-\frac{E_n}{\mu_n}t}\right]. \quad (6)$$

E_n and μ_n, associated with the elastic modulus and apparent viscosity of the nth layer can be extracted in Eq. (6). The fitted parameters may also be recast into a set of relaxation times as:

$$\tau_n = \frac{\mu_n}{E_n}, \quad (7)$$

where τ_n is the nth relaxation time associated with the response. For this paper, only three viscous branches were required to effectively model the cell body as a triple-layered structure. The SLS model is a particular case of the GM model with only one viscous branch and, thus, only one exponential term such that:

$$F(t) = \frac{4}{3}\frac{\sqrt{R\delta_0^3}}{(1-\nu)}\left[E_R + E_1 e^{-\frac{E_1}{\mu_1}t}\right]. \quad (8)$$

As shown in Fig. 1C, the improvements in the GM model over the SLS model to provide a better fit for stress-relaxation curve are considerable, particularly the conformance to the early-time fast relaxation behavior demonstrated by the cells in their initial responses.

2.5. Statistical analysis and curve fitting procedure

Data analysis including the GM model fitting to the experimental data and calculation of elastic modulus, apparent viscosity, and relaxation time of the sub-domains was performed with MATLAB software. The fittings were performed using a nonlinear least squares method to minimize the squared residual error of each fit. The GM model was given initial conditions that promoted the effective selection of consecutive relaxation times to ensure that higher modes were not considered. Shapiro–Wilks tests were conducted to analyze the data for normality. Two sample-independent t-tests with a 95% confidence interval ($P < 0.05$) were used to assess the degree of statistical difference between the two sets of results.

3. Results

For both the MCF10A and MDA-MB-231 cell types, AFM tests were performed on a set of about 30 single cells for acquiring stress-relaxation curves. Care was taken with the large indentation depth to avoid puncturing or damaging the cell membrane. If puncturing occurs, the curve exhibits local saw tooth behavior. No such behavior was observed in the data. The profiles of the distribution of the elastic moduli, the apparent viscosities, and the relaxation times among the two cell types calculated for the whole cell and each of the three sub-domains are compared using a series of histograms in Fig. 2 and the mean (±SD) values are also summarized in Table 1.

The biomechanical properties corresponding to the whole cell body are approximated for both cell types by fitting the SLS model. The results in Table 1 show that the average elastic modulus and apparent viscosity values of MCF10A cells are 33% ($p < 0.001$) and 61% ($p < 0.0001$) larger than those of MDA-MB-231 cells, respectively, indicating that MCF10A cells are stiffer and more viscous than MDA-MB-231 cells. The histograms of measured elastic modulus and apparent viscosity compared between two cell types (Fig. 2A and B) reveal that MDA-MB-231 cells are mechanically more homogeneous with a more concentrated distribution in comparison to MCF10A cells with a broad distribution. These results are in agreement with previously reported measurements on the elasticity [2,3] and viscosity [25] of the malignant cell lines at a shallow indentation. However, here, an upward shift toward larger $E_{elastic}$ and $\mu_{viscoelastic}$ values are observed for both cell types which is because of the application of a deep indentation in the measurements [15].

The biomechanical properties of the sub-cellular domains i.e. elastic moduli, apparent viscosities, and relaxation times are estimated using the GM models which significantly improved the fitting quality to the experimental data compared to the SLS models as shown in Fig. 1C. The data in Table 1 show there is a statistically significant ($p < 0.0001$) decreases in these values from up to low sub-domains, regardless of cell type. The up sub-domain corresponding to the cell membrane/cortex, is softer and extremely less viscous relative to the mid and low sub-domains.

Table 1 also shows how the biomechanical properties of sub-domains compare between normal and cancerous breast cells. In the up sub-domain, the biomechanical properties are fairly similar

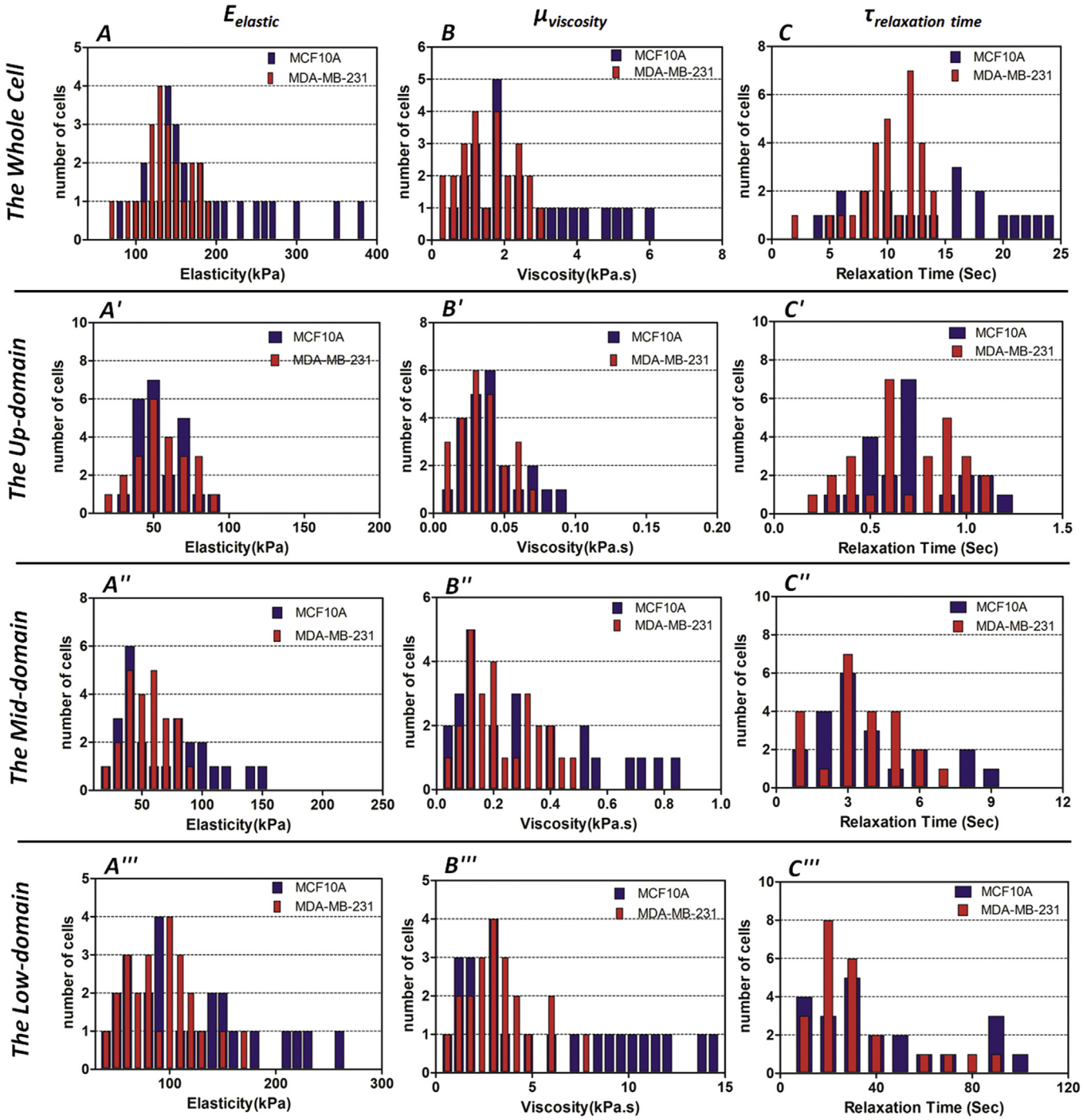

Fig. 2. Histograms of MCF10A and MDA-MB-231 cells depict the changes in distribution of measured elastic modulus (A, A′, A″, A‴), apparent viscosity (B, B′, B″, B‴), and relaxation time (C, C′, C″, C‴) for the whole cells and three sub-domains of the cells.

Table 1
Summary of elastic modulus, viscoelastic, and relaxation time responses for the whole and three sub-domains of normal and cancer cells.

Mean ± SD	Cell type	Whole cell	Up-domain of cell	Mid-domain of cell	Low-domain of cell
$E_{elastic}$ (kPa)	*MCF10A*	181.7 ± 73.4	58.97 ± 16.57	71.2 ± 39.74	127.8 ± 69.6
	MDA-231	136.4 ± 31.8	53.74 ± 18.04	61.9 ± 20.44	90.4 ± 36.8
$\mu_{viscoelastic}$ (kPa. s)	*MCF10A*	2.57 ± 1.52	0.046 ± 0.015	0.309 ± 0.255	5.85 ± 4.54
	MDA-231	1.59 ± 0.72	0.041 ± 0.015	0.247 ± 0.137	3.25 ± 1.86
$\tau_{relaxation\ time}$ (Sec.)	*MCF10A*	14.14 ± 6.12	0.78 ± 0.26	4.34 ± 2.51	45.78 ± 31.48
	MDA-231	11.65 ± 2.43	0.76 ± 0.24	3.98 ± 1.89	35.90 ± 22.37

in the normal MCF10A and malignant MDA-MB-231 cells. Here, the average values of the elastic modulus and the apparent viscosity were only slightly 9% ($p \approx 0.8$) and 11% ($p \approx 0.2$) less in the cancer cells, respectively, and this differences are statistically insignificant. In contrast, for the mid and low sub-domains corresponding to the cell cytoskeleton/nucleus and nuclear/integrin sub-domains, respectively, the difference in the biomechanical properties is more significant between the normal and cancer cells. For the mid and low sub-domains, the average elastic moduli of the cancer cells are, respectively, 13% ($p < 0.1$) and 29% ($p < 0.01$) less than that of normal cells. Similarly, the average apparent viscosities of the mid and low sub-domains are 20% ($p < 0.01$) and 44% ($p < 0.001$) less in the cancer cells compared to the normal cells, respectively. Conclusively, the deeper indentation which probes the internal structural sub-domains is more sensitive to mechanically differentiating normal and cancer cells than a typical shallow indentation.

We also analyzed the relaxation times which is a measure of stress-relief under a constant deformation. The average relaxation time measurements for the whole cell and the three sub-domains in Table 1, show an overall decrease in this parameter from the normal to the cancer cells, which, however, are statistically insignificant.

The distributions of the elastic moduli (Fig. 2A′) and the apparent viscosities (Fig. 2B′) calculated for the up sub-domain reveal they are similar for the normal and cancer cells consistent with population data summarized in Table 1. However, for the mid and low sub-domains, the distributions of the two cell types are distinct for $E_{elastic}$ (Fig. 2A″ and A‴) and $\mu_{viscoelastic}$ (Fig. 2B″ and B‴). The normal MCF10A cells exhibited a broader distribution through the larger $E_{elastic}$ and $\mu_{viscoelastic}$ values, than that of the cancerous MDA-MB-231. The histograms of the relaxation time shown in Fig. 2C, C′, 2C″, and 2C‴ also showed a slight shift toward larger time for normal cells compared to cancer cells.

Morphological analyses were performed to confirm the dimensions of the cells used in the calculations. Scanning electron microscopy (SEM) images were used to directly measure the height of the cells, (Fig. 3A, MDA-MB-231; Fig. 3B, MCF10A). The average values taken from 12 samples measurements in each cell type indicate that the MDA-MB-231 cells have a thickness of about 5.71 μm while MCF10A cells are about 6.66 μm thick.

4. Discussion

The simple models that assume the cell body as a homogeneous solid can be extended to a multi-layered model for biomechanical characterization of the cells. The multi-modal response of both MCF10A and MDA-MB-231 cells and the biomechanical parameters reflect the cell heterogeneity across the body. By recognizing that living cells behave mechanically as a multi-layered structure, the presented force microscopy analysis provides valuable information about the biomechanics of the different sub-cellular structures that are located in different depths.

As the AFM tip indents deeper into the cell, it perturbs various cellular structures that respond differently to a mechanical stimulus. Our results show, for a deep indentation, the elastic modulus and the apparent viscosity are higher when compared to a shallow indentation scenario, and this can possibly be attributed to the effects of a stiff and viscous inner cytoplasmic layer and nucleus [15]. However, when using models that assume a homogeneous cell body, the mechanical changes occurring at different depths of the cell are averaged. An important finding in our work is that a shallow indentation that exerted biomechanical actions in the cell relatively localized to the up sub-domain revealed relatively modest differences between the normal and malignant cells. However, the responses of normal and malignant cells differed quite significantly when a deep indentation was applied. As a note, using a modified AFM needle penetration technique, it was demonstrated in another recent study that nuclei and also membrane/cytoplasm of the highly metastatic bladder cancer cell line have significantly lower Young's moduli when compared to its less metastatic counterpart [26]. This result is in agreement with known oncogenic events that exert pleiotropic alterations in cytoskeleton and nuclear components, and the implication of this result is that use of deep, rather than shallow indentation might provide a more robust probe of the progression of normal cells to malignancy.

The assignment of the three sub-domains to an outer membrane/cortex, a central cytoplasm/nucleus, and an inner nuclear/integrin can be verified by correlating the corresponding measurements to the literature values. The results of previous studies show there is a continuum of biological elements which establish a mechano-transduction cascade linking membrane displacements to cytoskeletal filaments, the nucleus and sub-nuclear structures, and cell integrin-substrate forces [27,28]. Thus, the biomechanical measurements cannot be assigned to a particular sub-structure, but dominated by the response of a sub-cellular structural domain. The term ‘cortex’ refers to a cortical actin layer, located right underneath the membrane [29,30]. The term ‘cytoplasm’ is attributed to the intracellular cytoskeletal proteins composed mainly of actin filaments, intermediate filaments, and microtubules. Importantly, the previously reported time constants for the cell membrane/cortex (milli-second), the cell cytoskeleton (second), and the cell nucleus (10-second) [29,31] in the literature are of the same order as the relaxation times extracted by the GM model measurements in Table 1 for the three sub-domains. Notably, a recent AFM-based work has measured the viscosity of the membrane/cortex (0.081 ± 0.018 kPa s) and cytoplasm (0.720 ± 0.161 kPa s) for breast MCF-7 cells using the GM model [22]. The viscosity measurement of the chondrocyte cell nucleus (~4–5 kPa s) was also measured by applying the GM model to the micropipette aspiration data [31]. The results presented in Table 1 for three different sub-cellular domains are in good agreement with the previously reported data.

Together, the approach outlined here can be used as a powerful tool to investigate the biomechanical properties of sub-cellular structures as biomechanical signature of malignancy, metastatic potential, and anti-cancer drug sensitivity and drug resistance.

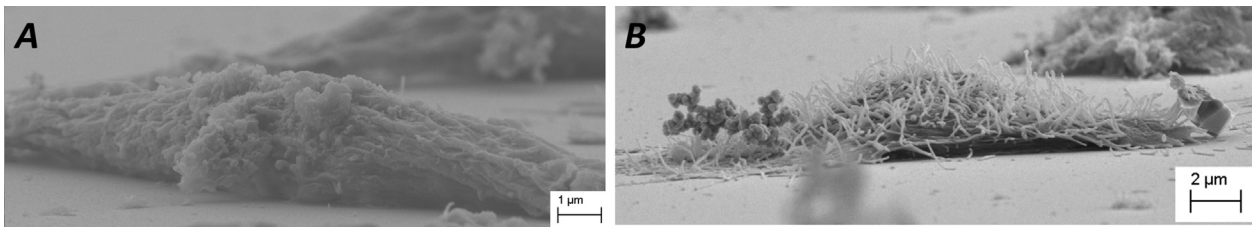

Fig. 3. SEM side-view image of (A) MDA-MB-231 cell and (B) MCF10A cell.

Conflict of interest

None.

Acknowledgments

The research is funded by the National Science Foundation under award number CBET-1403304 and ECCS-0925945 (to MA), and the University of Alabama RGC award (to SNM). The authors would like to thank the Fralin life science institute at Virginia Tech for equipment support.

Transparency document

Transparency document related to this article can be found online at http://dx.doi.org/10.1016/j.bbrc.2015.05.100.

References

[1] S. Suresh, Biomechanics and biophysics of cancer cells, Acta Biomater. 3 (2007) 413–438.
[2] M. Nikkhah, J.S. Strobel, R. De Vita, M. Agah, The cytoskeletal organization of breast carcinoma and fibroblast cells inside three dimensional isotropic silicon microstructures, Biomaterials 31 (2010) 4552–4561.
[3] M. Nikkhah, J.S. Strobl, E.M. Schmelz, M. Agah, Evaluation of the influence of growth medium composition on cell elasticity, J. Biomechanics 44 (2011) 762–766.
[4] B. Lincoln, H.M. Erickson, S. Schinkinger, F. Wottawah, D. Mitchell, S. Ulvick, C. Bilby, J. Guck, Deformability-based flow cytometry, Cytom. Part A 59 (2004) 203–209.
[5] R. Zhao, K. Wyss, C. Simmons, Comparison of analytical and inverse finite element approaches to estimate cell viscoelastic properties by micropipette aspiration, J. Biomechanics 42 (2009) 2768–2773.
[6] M. Sato, D.P. Theret, L.T. Wheeler, Application of the micropipette technique to the measurement of cultured porcine aortic endothelial cell viscoelastic properties, J. Biomech Eng. 112 (1990) 263–268.
[7] E.L. Elson, Cellular mechanics as an indicator of cytoskeletal structure and function, Annu. Rev. Biophys Biophys Chem. 17 (1988) 397–430.
[8] E.M. Darling, S. Zauscher, F. Guilak, Viscoelastic properties of zonal atricular chondrocytes measured by atomic force microscopy, Osteoarthr. Cartil. 14 (2006) 571–579.
[9] E.M. Darling, S. Zauscher, J.A. Block, F. Guilak, A thin-layer model for viscoelastic, stress-relaxation testing of cells using atomic force microscopy: do cell properties reflect metastatic potential? Biophys J. 92 (2007) 1784–1791.
[10] E.M. Darling, M. Topel, S. Zauscher, T.P. Vail, F. Guilak, Viscoelastic properties of human mesenchymally-derived stem cells and primary osteoblasts, chondrocytes, and adipocytes, J. Biomechanics 41 (2008) 454–464.
[11] Q.S. Li, G.Y.H. Lee, C.N. Ong, C.T. Lim, AFM indentation study of breast cancer cells, Biochem. Biophys Res. Commun. 374 (2008) 609–613.
[12] G. McPhee, M.J. Dalby, M. Riehle, H. Yin, Can common adhesion molecules and microtopography affect cellular elasticity? A combined atomic force microscopy and optical study, Med. Biol Eng. Comput. 48 (2010) 1043–1053.
[13] I.D. Medalsy, D.J. Muller, Nanomechanical properties of proteins and membranes depend on loading rate and electrostatic interactions, ACS Nano 7 (2013) 2642–2650.
[14] T. Tsui, G. Pharr, Substrate effects on nanoindentation mechanical property measurement of soft films on hard substrate, J. Mater. Res. 14 (1999) 292–301.
[15] M. Zhao, C. Srinivasan, D.J. Burgess, B.D. Huey, Rate- and depth-dependent nanomechanical behavior of individual living Chinese hamster ovary cells probed by atomic force microscopy, J. Mater. Res. 21 (2006) 1906–1912.
[16] A.B. Mathur, A.M. Collinsworth, W.M. Reichert, W.E. Kraus, G.A. Truskey, Endothelial, cardiac muscle and skeletal muscle exhibit different viscous and elastic properties as determined by atomic force microscopy, J. Biomechanics 34 (2001) 1545–1553.
[17] S. Kasas, X. Wang, H. Hirling, R. Marsault, B. Huni, A. Yersin, R. Regazzi, G. Grenningloh, B. Riederer, L. Forro, G. Dietler, S. Catsicas, Superficial and deep changes of cellular mechanical properties following cytoskeleton disassembly, Cell Motil. Cytoskelet. 62 (2005) 124–132.
[18] T.K. Chang, Y.A. Rossikhin, M.V. Shitikova, Application of fractional-derivative standard linear solid model to impact response of human frontal bone, Theor. Appl. Fract. Mech. 56 (2011) 148–153.
[19] H. Liu, D.P. Noonan, Y.H. Zweiri, The development of nonlinear viscoelastic model for the application of soft tissue identification, in: IEEE/RSJ International Conference on Intelligent Robots and Systems, 2007, pp. 208–213.
[20] J. Shen, C. Li, H. Wu, Fractional order viscoelasticity in characterization for atrial tissue, Korea-Australia Rheology J. 25 (2013) 87–93.
[21] B. Wang, P. Lançon, C. Bienvenu, A general approach for the microrheology of cancer cells by atomic force microscopy, Micron 44 (2013) 287–297.
[22] S. Moreno-Flores, R. Benitez, M. dM Vivanco, J.L. Toca-Herrera, Stress relaxation and creep on living cells with the atomic force microscope: a means to calculate elastic moduli and viscosities of cell components, Nanotechnology 21 (2010) 445101.
[23] M.O. Krisenko, A. Cartagena, A. Raman, R.L. Geahlen, Nanomechanical property maps of breast cancer cells as determined by multiharmonic atomic force microscopy reveal Syk- dependent changes in microtubule stability mediated by MAP1B, Biochemistry 54 (2015) 60–68.
[24] H. Hertz, On the contact of elastic solids, J. Reine Angew Math 92 (1881) 156–171.
[25] A.N. Ketene, E.M. Schmelz, P.C. Roberts, M. Agah, The effects of cancer progression on the viscoelasticity of ovarian cell cytoskeleton structures, Nanomedicine : Nanotechnol. Biol. Med. 8 (2011) 93–102.
[26] H. Liu, J. Wen, Y. Xiao, J. Liu, S. Hopyan, M. Radisic, C.A. Simmons, Y. Sun, In situ mechanical characterization of the cell nucleus by atomic force microscopy, ACS NANO 8 (2014) 3821–3828.
[27] N. Wang, J.D. Tytell, D.E. Ingber, Mechanotransduction at a distance: mechanically coupling the extracellular matrix with the nucleus, Nat. Rev. Mol. Cell. Biol. 10 (2009) 75–82.
[28] K.M. Imbalzano, N. Cohet, Q. Wu, J.M. Underwood, A.N. Imbalzano, J.A. Nickerson, Nuclear shape changes are induced by knockdown of the SWI/SNF ATPase BRG1 and are independent of cytoskeletal connections, PLoS One 8 (2013) e55628.
[29] H. Karcher, J. Lammerding, H. Huang, R.T. Lee, R.D. Kamm, M.R. Kaazempur-Mofrad, A three-dimensional viscoelastic model for cell deformation with experimental verification, Biophys J. 85 (2003) 3336–3349.
[30] T. Kazutaka, T. Takehito, M. Ryusuke, N. Ichiro, M. Takuro, O. Aiji, Human erythrocytes possess a cytoplasmic endoskeleton containing β-actin and neurofilament protein, Archives Histology Cytol. 69 (2006) 329–340.
[31] F. Guilak, J.R. Tedrow, R. Burgkart, Viscoelastic properties of the cell nucleus, Biochem. Biophys Res. Commun. 269 (2000) 781–786.
[32] H. Babahosseini, A.N. Ketene, E.M. Schmelz, P.C. Roberts, M. Agah, Biomechanical profile of cancer stem-like/tumor-initiating cells derived from a progressive ovarian cancer model, Nanomed. Nanotechnol. Biol. Med. 10 (2014) 1013–1019.
[33] H. Babahosseini, P.C. Roberts, E.M. Schmelz, M. Agah, Bioactive sphingolipid metabolites modulate ovarian cancer cell structural mechanics, Integr. Biol. 5 (2013) 1385–1392.
[34] B. Carmichael, H. Babahosseini, S.N. Mahmoodi, M. Agah, The fractional viscoelastic response of human breast tissue cells, Phys. Biol. 12 (2015) 046001.